IEEE Access
Multidisciplinary | Rapid Review | Open Access Journal

Received July 17, 2019, accepted August 10, 2019, date of publication August 13, 2019, date of current version August 28, 2019.

Digital Object Identifier 10.1109/ACCESS.2019.2935129

MEMS Accelerometer Calibration Denoising Method for Hopkinson Bar System Based on LMD-SE-TFPF

ZEYU YAN[1], BOYANG HOU[2], JINGCHUN ZHANG[3], CHONG SHEN[1], YUNBO SHI[1], JUN TANG[1], HUILIANG CAO[1], (Member, IEEE), AND JUN LIU[1]

[1]Science and Technology on Electronic Test and Measurement Laboratory, North University of China, Taiyuan 030051, China
[2]Glasgow College, University of Electronic Science and Technology of China, Chengdu 610054, China
[3]Beijing Huijia Private School, Beijing 102200, China

Corresponding authors: Huiliang Cao (caohuiliang1986@126.com) and Jun Liu (liuj@nuc.edu.cn)

This work was supported in part by the National Natural Science Foundation of China under Grant 51705477, Grant 61603353, and Grant 61703098, in part by the Pre-Research Field Foundation of Equipment Development Department of China under Grant 61405170104, in part by the Program for the Top Young Academic Leaders of Higher Learning Institutions of Shanxi, in part by the Fund Program for the Scientific Activities of Selected Returned Overseas Professionals in Shanxi Province, in part by the Shanxi Province Science Foundation for Youths under Grant 201801D221195, in part by the Young Academic Leaders of North University of China under Grant QX201809, in part by the Fund of Science and Technology on Electronic Test and Measurement Laboratory under Grant WD614200104011804, in part by the Weapons and Equipment Joint Fund under Grant 6141B021304, and in part by the Fund for Shanxi "1331 Project" Key Subjects Construction.

ABSTRACT High-G MEMS accelerometer (HGMA) is widely used in the aerospace field and the precise control of missiles. Therefore, its calibration accuracy is critical to sensor performance and the overall control system. In order to decrease the influence of noise on the HGMA output signal, a hybrid denoising algorithm which is based on the Time-frequency peak filtering (TFPF), Local mean decomposition (LMD) and Sample entropy (SE) has been proposed in this article. For the problem that the TFPF algorithm is limited in the choice of window length, LMD and SE are used to distinguish components, which can improve the TFPF algorithm effectively. It provides a better balance between noise reduction and signal fidelity. Firstly, the noise-containing signal can be decomposed by LMD to obtain PFs. Secondly, calculate the sample entropy values of each PFs, then divide the signal into mixed component, useful component and noise component according to the similarity of sample entropy. Thirdly, the mixed component can use long-window TFPF to reduce noise, the short-window TFPF can reduce the noise for the useful component, and the noise component can be wiped off directly. Finally, the useful component and the mixed component are both reconstructed to form the final denoised signal. Experiments have showed that this method can not only remove noise (the noise of static signal is reduced by 91.76%, the signal-noise ratio of dynamic signal has increased to 17.6), but also retain the details of frequency and amplitude (the shock peak amplitude error is 0.062% and the vibration amplitude error is 0.04%). Therefore, this method can reduce the noise of the High-G MEMS accelerometer signal with maintaining the characteristics of the original signal, thereby greatly improves the performance of the accelerometer, making it widely used.

INDEX TERMS High-G MEMS accelerometer (HGMA), denoising, local mean decomposition (LMD), sample entropy (SE), time-frequency peak filtering (TFPF), Hopkinson bar.

I. INTRODUCTION

Since the MEMS inertial sensors are widely used in the aerospace, weapon equipment and consumer electronics fields [1]–[6], the High-G MEMS accelerometer (HGMA) has come to a new type of sensor developed by microelectronics and micromachining technology. Compared with ordinary accelerometers, it has the advantages of light weight, small size, high integration density, high reliability, etc. However, due to the inevitable causes of hardware circuits and sensors, the HGMA output signal contains a lot of noise, which could seriously affect the accuracy of the calibration. Therefore,

The associate editor coordinating the review of this article and approving it for publication was Flavia Grassi.

This work is licensed under a Creative Commons Attribution 4.0 License. For more information, see http://creativecommons.org/licenses/by/4.0/

reducing the noise of the HGMA output signal can improve the its performance [7], [8].

Although there are some excellent denoising algorithms now, such as Wavelet transform, Fourier transform, Empirical mode decomposition (EMD), Local mean decomposition (LMD), Time-frequency peak filtering (TFPF), Morphological filter (MF), varying degrees of deficiencies still exist. The Wavelet transform is a time-frequency analysis method [9], [10]. It can characterize local features of the signal in both time and frequency domains. Known as a microscope for analyzing processed signals, The Wavelet transform is very suitable for extracting local features of a complex signal. The Wavelet threshold denoising is an effective denoising method based on wavelet transform. It uses the different characteristics of the effective signal and random noise after wavelet transform distinguishes the two, so as to achieve the purpose of noise reduction [11]. However, with some certain defects, the traditional hard threshold wavelet transform can cause mutations in the wavelet domain and finally resulting in local jitter after denoising. The Fourier transform is one of the most common and basic methods in signal analysis [12]. Being a frequency domain analysis method, it can well characterize the frequency characteristics of a signal. However, it can't provide any time domain information, which means that it lacks of positioning when it is applied to the time domain. Proposed by Dr. Norden Huang, an American engineering academician, Empirical mode decomposition (EMD) is an adaptive data processing method, which is very suitable for nonlinear, non-stationary time series processing [13]–[15]. But this method still has difficulties that have not been overcome, such as modal aliasing. Put forward by Jonathan S. Smith, Local mean decomposition (LMD) is an adaptive time-frequency analysis method that can adaptively decomposes complex signals into a set of product functions (PFs) [16]–[18].Comparing the comparison of EMD with LMD, we can see that LMD is more superior to EMD in many respects [15]. In addition, Time-frequency peak filtering (TFPF) is an effective denoising method which has been widely used, but TFPF has contradictions in the choice of window length [19]–[21]. When the long window is selected, the random noise can be effectively reduced, but the signal amplitude is severely attenuated. While when the short window length is used, the amplitude of the effective signal is well maintained, but the noise would not be well reduced.

In recent years, the hybrid denoising algorithms have gradually emerged and they are widely used in different fields. A large number of experimental results have shown that the hybrid denoising algorithm usually works better than a single algorithm [22]–[36]. Lv and Yu introduced an average combined differential morphological filter for feature extraction, where the scale selection of structural elements was determined by Teager energy kurtosis (TEK) [29]. The traditional MF algorithm is easy to be disturbed. Hu *et al.* proposed an improved MF algorithm to overcome the shortcomings of traditional MF [30]. Xu *et al.* proposed a new wavelet threshold denoising method, which can obtain the best estimation in Besov space [31]. Bi *et al.* combined EMD and wavelet transform and applied it to the detection of engine blasting characteristics [33]. This method is suitable for non-stationary engine knock signal, and can identify tapping characteristics of vibration signal, which is more reliable than previous signal processing methods. In order to reduce the noise signal measured from the gearbox, Ning et al. combined the Local mean decomposition and Time-frequency peak filtering to form a hybrid algorithm [21]. This method is obviously more reliable and more efficient than previous signal processing methods. In addition, Sample Entropy (SE) is used to calculate the complexity of PFs and then classify them according to SE values [24], [26], [38], [39].

In this paper, in order to improve the calibration accuracy of HGMA, Time-Frequency Peak Filtering method is well combined with Local mean decomposition, and Sample entropy (SE) is introduced to divide the signal into useful component, mixed component, and pure noise component. The pure noise component can be wiped off directly, the mixed component is easily denoised with a long-window TFPF to reduce random noise, and the useful component is denoised with a short-window TFPF so that the amplitude of the effective signal is well maintained [40]. Through a large number of simulation experiments, we have made corresponding improvements to the original method. Compared with reducing the noise of the mixed signal as a whole, we found that separate denoising is more effective after dividing the test signal into static output and dynamic output. Because the static signal and the dynamic signal have different frequency and amplitude characteristics, the local mean decomposition is more accurate after dividing the test signal into static output and dynamic output. This paper have optimized the parameters (window length of TFPF) for the accelerometer's high-g working environment, at the same time, the high frequency characteristic of the signal is considered. This paper have analyzed not only the amplitude of the signal during the shock process, but also the performance of different denoising methods in the vibration stage. In addition, this article have also tested the denoising effect with the Allan variance, thereby better verifying the reliability of the noise reduction method. Experimental results can verify the advantages of the hybrid denoising method proposed in this paper. The noise of static signal is reduced by 91.76%, the signal- noise ratio [41] of dynamic signal has increased to 17.6, the shock peak amplitude error is 0.062% and the vibration amplitude error is 0.04% [42], [43]. This hybrid denoising method is suitable for the removal of high-g MEMS accelerometer signals with shock and vibration characteristics.

In order to improve the performance of accelerometer during High-G calibration, a hybrid denoising algorithm based on LMD, SE and TFPF is proposed in this paper. The rest of this paper is organized as follows: Section 2 is a description of the proposed LMD-SE-TFPF algorithm. Accelerometer description and experimental results are shown in Section 3;

Section 4 is the discussion of denoising result; Section 5 is the conclusion.

II. METHODS

A. LOCAL MEAN DECOMPOSITION (LMD)

Local mean decomposition (LMD) is an adaptive signal decomposition method, which can decompose a complex non-stationary signal into a set of product function (PF) adaptively. Obtained by multiplying the envelope signal and the frequency modulation signal, PF represents the instantaneous amplitude of the envelope signal and its instantaneous frequency is obtained from the purely frequency modulated signal. Therefore, the complete time-frequency distribution of the original signal can be obtained by combining the transient parameters of the respective PF components. The product function generated by the LMD can store more frequency and envelope information than the eigenmode function generated by EMD.

The process of decomposition for any non-stationary signal is shown as follows [17]:

- Step 1: Find all the extreme points p_i of the signal.
- Step 2: Find the local mean function $m_i(t)$ of the signal and the local envelope function $a_i(t)$ according to the extreme points of the signal. The local mean function of each segment is given by the following formula:

$$m_i = (p_i + p_{i+1})/2 \tag{1}$$
$$a_i = |p_i - p_{i+1}|/2 \tag{2}$$

An important step in the LMD is to use the moving average method, which can obtain the mean and amplitude of the envelope. While the local mean function and the local envelope function of the signal are obtained by mi and ai. After the moving average processing, a smoothed local mean function $m_{11}(t)$ and a local envelope function $a_{11}(t)$ are obtained. The span of the moving average selects one-third of the maximum distance between adjacent extreme points. The sequences to be smoothed are $m_i(t)$ and $a_i(t)$, span is $2k + 1$, where k is a positive integer. The calculation formula of the moving average is:

$$\begin{cases} m_{11}(t) = \dfrac{1}{2k+L}[m_1(t-k) + \cdots m_1(t) + \cdots m_1(t+k)] \\ a_{11}(t) = \dfrac{1}{2k+L}[a_1(t-k) + \cdots a_1(t) + \cdots a_1(t+k)] \end{cases} \tag{3}$$

- Step 3: Separate the smoothed local mean function from the original signal x(t), and obtain the $h_{11}(t)$:

$$h_{11}(t) = x(t) - m_{11}(t) \tag{4}$$

- Step 4: In order to demodulate $h_{11}(t)$, divide $h_{11}(t)$ by $a_{11}(t)$ to obtain:

$$s_{11}(t) = \frac{h_{11}(t)}{a_{11}(t)} \tag{5}$$

- Step 5: Find the local envelope function $a_{12}(t)$. If $a_{12}(t) = 1$, then $S_{11}(t)$ is already the frequency modulated signal, otherwise repeat $S_{11}(t)$ as the original data until $a_{1(n+1)}(t) = 1$. Then have:

$$\begin{cases} h_{11}(t) = x(t) - m_{11}(t) \\ h_{12}(t) = s_{11}(t) - m_{11}(t) \\ \qquad \vdots \\ h_{1n}(t) = s_{1(n-1)}(t) - m_{1n}(t) \end{cases} \tag{6}$$

Among them:

$$\begin{cases} s_{11}(t) = h_{11}(t)/a_{11}(t) \\ s_{12}(t) = h_{12}(t)/a_{12}(t) \\ \qquad \vdots \\ s_{1n}(t) = h_{1n}(t)/a_{1n}(t) \end{cases} \tag{7}$$

- Step 6: Multiply all the local envelope functions which are generated by the above process, the corresponding envelop is given by:

$$a_1(t) = a_{11}(t) \cdot a_{12}(t) \cdots = \prod a_{1q}(t) \tag{8}$$

- Step 7: The envelope signal and the frequency modulated signal are multiplied to obtain a first PF component PF1 of the original signal, the frequency modulation signal is $S_{1n}(t)$.

$$PF_1(t) = a_1(t) \cdot s_{1n}(t) \tag{9}$$

It contains the highest frequency component of the original signal, which is a single component AM-FM signal. Its instantaneous amplitude is the envelope signal $a_1(t)$, and its instantaneous frequency $f_{1n}(t)$ is obtained from the pure frequency modulated signal $S_{1n}(t)$. Which is:

$$f_{1n}(t) = \frac{1}{2\pi} \cdot \frac{d[\arccos(s_{1n}(t))]}{dt} \tag{10}$$

- Step 8: The first PF component PF1(t) is subtracted from the signal X(t) to obtain a new signal $h_{11}(t)$. Repeat the above steps n times using $h_{11}(t)$ as the new source data until $h_{1n}(t)$ becomes a monotonic function. At this time, the number of PFs is determined to be n.

$$x(t) = \sum_{k=1}^{n} PF_k(t) + h_{1n}(t) \tag{11}$$

Local mean decomposition is a process of gradually removing the high-frequency components of the signal, which can be seen from the specific steps of LMD. The decomposition process consists three layers cycles: the moving average of the local mean function and the local envelope function, obtaining the PF component and the process of finding all PF components and residual components.

B. SAMPLE ENTROPY (SE)

After the local mean decomposition, the original signal is decomposed into a large number of PFs. This paper introduce the Sample entropy (SE) to divide PFs into different components, making the denoising process more targeted. Being an improved method for measuring the complexity of time series based on approximate entropy, Sample entropy detects time series of similar periods and calculates a non-negative number for the sequence. The larger the value, the more complex the data.

Sample entropy is defined as [25]:

$$SampEn(N, j, r) = \lim_{N\to\infty} \{\ln[\frac{1}{N-j+1}\sum_{i=1}^{N-j+1} C_r^j(i) - \frac{1}{N-(j+1)+1}\sum_{i=1}^{N-(j+1)+1} C_r^{j+1}(i)]\} \tag{12}$$

Since the actual calculation application process N cannot be infinite, so when N takes a finite value:

$$SampEn(N, j, r) = \ln[\frac{1}{N-j+1}\sum_{i=1}^{N-j+1} C_r^j(i) - \frac{1}{N-(j+1)+1}\sum_{i=1}^{N-(j+1)+1} C_r^{j+1}(i)] \tag{13}$$

where N is the length of the signal; j is the length of the match, also called embedded dimension, it usually takes a value of 1 or 2; r is the probability that any two time points match each other, called similar tolerance (usually selecting 10%-25% of the signal standard deviation).

C. TIME-FREQUENCY PEAK FILTERING (TFPF)

In recent years, the Time-frequency peak filtering algorithm has been widely used in signal processing as a noise cancellation technology. It is a signal enhancement method based on the pseudo-Wiener-Ville distribution (PWVD) to better estimate instantaneous frequency of the data, which uses the time-frequency distribution peak of the frequency-modulated signal as an instantaneous frequency estimate to reduce random noise. Wiener-Ville distribution (WVD) is a bilinear time-frequency distribution with good time-frequency focusing, but its performance is reduced due to cross terms when dealing with multi-component signals. Pseudo-Wiener-Ville distribution (PWVD) is an effective method for suppressing cross terms in WVD. TFPF algorithm first needs to encode the signal into an analytical signal of the instantaneous frequency, and then estimate the instantaneous frequency of analytical signal as the estimate of the effective signal.

The output signal x(t) of the accelerometer can be expressed as:

$$x(t) = y(t) + n(t) \tag{14}$$

where: y(t) is the effective signal in the output signal, n(t) is the noise.

The steps to remove the noise of the accelerometer output signal using Time-frequency peak filtering are as follows [19]:

- Step 1: The signal x(t) is encoded by frequency modulation:

$$z(t) = e^{j2\pi\mu\int_0^t x(\lambda)d\lambda} \tag{15}$$

  Here, μ is the frequency modulation index. The noisy signal x(n) is converted into the instantaneous frequency of the analytic signal z(t).
- Step 2: Calculate the pseudo-Wigner-Ville distribution spectrum of the analytical signal z(t).

$$PW_z(t, f) = \sum_{m=-\infty}^{\infty} h(m)z(t+m)z^*(t-m)e^{-j4\pi fm} \tag{16}$$

  where, z∗ is the conjugate operator to z, f is frequency of the signal. The length of the window function h(m) is a parameter that affects the tradeoff between noise attenuation and signal preservation.
- Step 3: Then, the peak value of the pseudo-Wiener-Ville distribution (PWVD) of z(t) is used to estimate the effective signal y(t). Take the maximum value of PWVD to obtain the instantaneous frequency estimate:

$$f_z(t) = \frac{\arg\max[PW_z(t, f)]}{\mu} \tag{17}$$

  where argmax[.] is the operator that takes the maximum value along the frequency direction, $f_z(t)$ is the instantaneous frequency function.

The size of the window length in the TFPF directly affects the effect of signal fidelity and noise reduction. After the long-window length TFPF noise reduction, the denoising effect of the signal is good, but there will be some loss in amplitude, especially in the position of the peak and trough. The attenuation of signal amplitude is small after TFPF denoising with short-window length, however, there are still many noise components. Different signal components are denoised by different window length TFPF after Local mean decomposition and classification, which not only preserves the effective signal, but also effectively removes random noise.

D. INTRODUCTION OF LMD-SE-TFPF

In order to solve the limitation of TFPF in window length selection, Local mean decomposition, Sample entropy and Time-frequency peak denoising algorithm are all combined.

- Step 1: Local mean decomposition
  Local mean decomposition is performed on the load output signal to obtain different PFs of the instantaneous high-frequency components. However, each PF component is not a pure noise mode or a pure signal mode, but a mode in which useful component and noise component are mixed. Therefore, it is not possible to directly discard

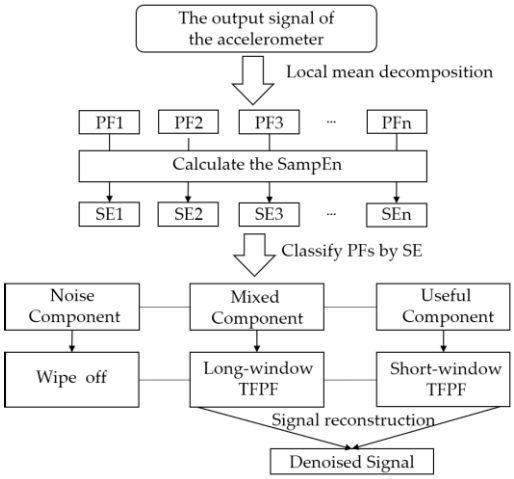

FIGURE 1. The steps of LMD-SE-TFPF algorithm.

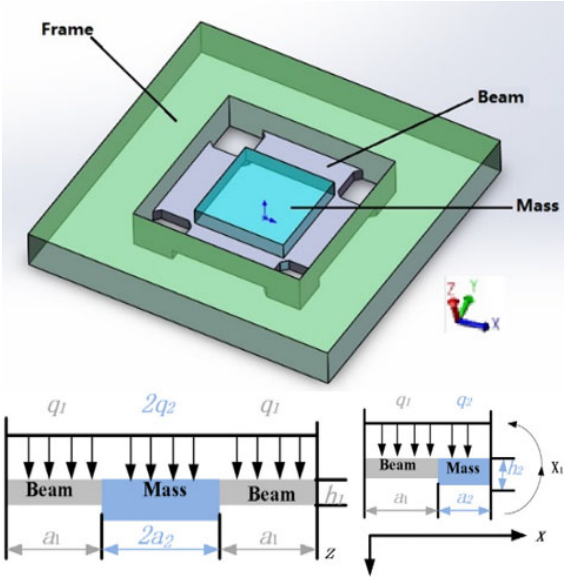

FIGURE 2. HGMA structure schematic and size.

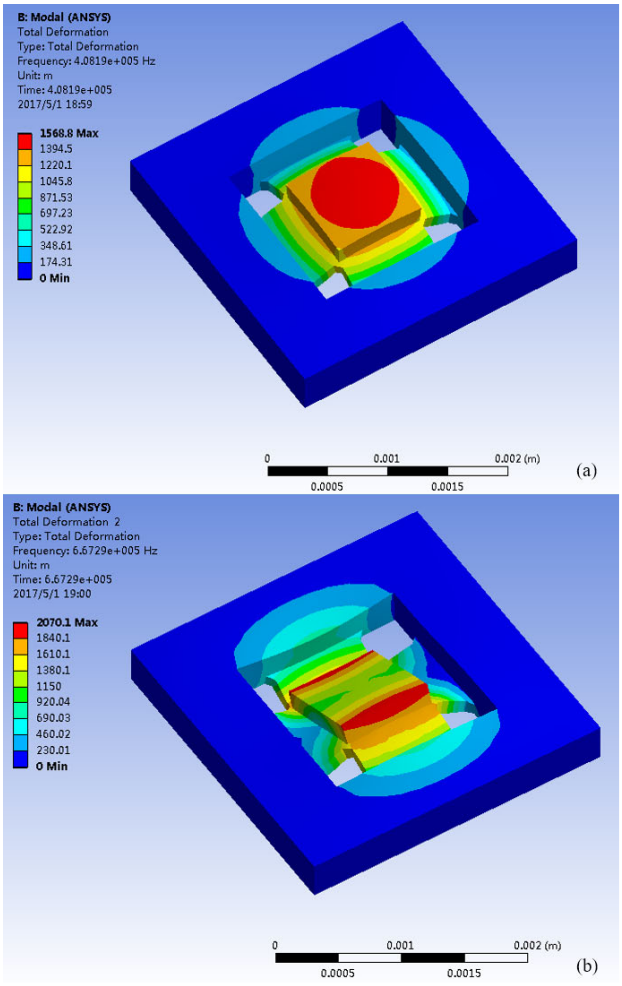

FIGURE 3. Mode simulation of HGMA structure (a) (b) are 1st and 2nd order modes.

the mode dominated by noise or retain the dominant mode of the signal. We need to use the sample entropy to calculate the similarity of each PFs, and then determine which modes need to be denoised.

- Step 2: Calculate SE and classify
  SE characterizes the complexity of an unsteady time series. Its core idea is to detect the probability of a new subsequence appearing in a time series. In the LMD-SE-TFPF algorithm, the SE value of each PF component is calculated to distinguish the complexity of each PF component, and the PFs are classified according to the similarity of SE values, which are divided into three parts on average. PFs in the minimum interval is considered as a useful component, while in the middle range, it is considered as a mixed component, and pure noise component is in the largest interval. The ideal useful component is a pure signal with no noise, the noise component should be pure noise, and the mixed component contains pure signal and pure noise. Therefore, the useful component needs to be well preserved, the mixed component needs to be denoised, and the noise component is wiped off.
- Step 3: Denoise for different signal components
  Select TFPF with different window length to denoise for the signal components. Due to the denoising effect is better after long-window length TFPF, so the mixed component is denoised by the long-window length TFPF. The attenuation of signal waveform and amplitude is small after denoising by short-window length TFPF, so the useful component is denoised by the short-window length TFPF. Finally, we remove the noise component directly. When we adjust the window length, its parameter is gradually increased until the signal is distorted. At this time, the maximum undistorted window length is the appropriate parameter.
- Step 4: Signal reconstruction
  Reconstruct the denoised mixed component and useful component, the final denoised signal is obtained. Signal

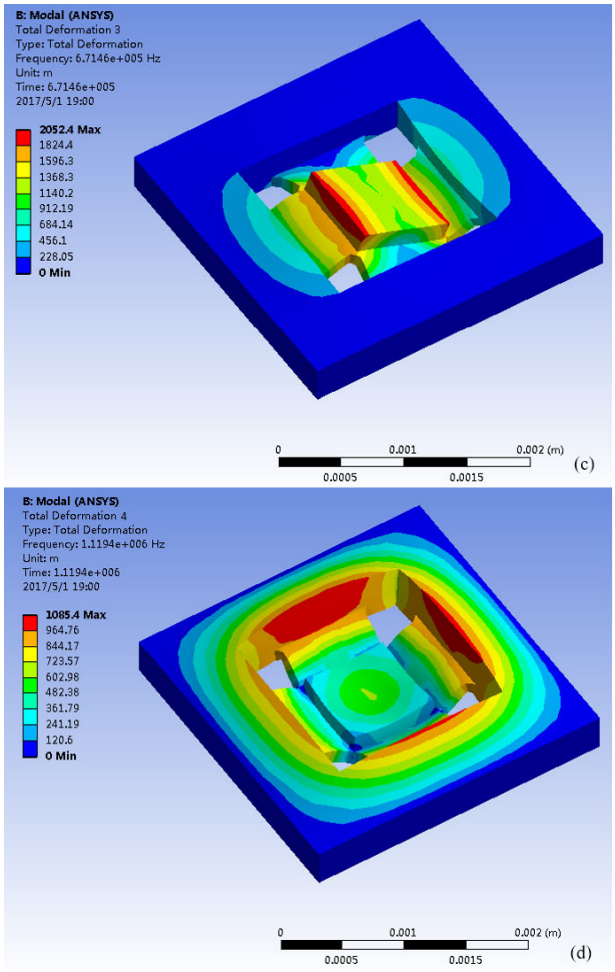

FIGURE 4. Mode simulation of HGMA structure (c) (d) are 3rd and 4th order modes.

reconstruction is actually a process of superimposing the denoised mixed components with the denoised useful components.

The steps of the LMD-SE-TFPF method are shown in Figure 1.

III. EXPERIMENT AND RESULTS

A. HIGH-G MEMS ACCELEROMETER

The original signal collected in this paper is from the High-G MEMS accelerometer (HGMA) which is a newly designed and manufactured sensor. It has the characteristics of high impact survival rate and high range. The working principle of HGMA is Piezoresistive effect, and the unit of the output signal is voltage. HGMA adopts four beams and island structure, as is shown in Figure 2. The frame, four beams and the center mass are all rectangles, which are good for processing.

The cross section of the accelerometer constructed the coordinate system. The central dividing line of the cross section is Z axis, and the specified direction is downward. The other middle line is the X axis, and the right direction is

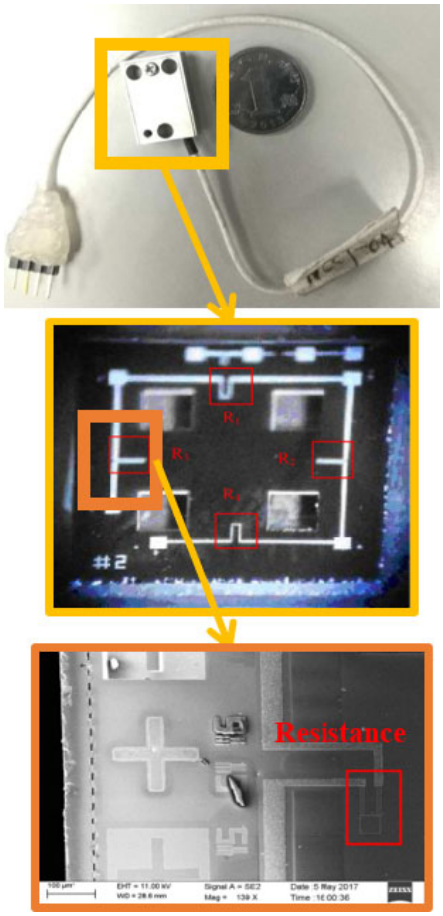

FIGURE 5. Overall photo, CCD photo and SEM photo of HGMA.

TABLE 1. Structural parameters of the HGMA.

	Beam			Mass		
Parameter	length (a_1)	width (b_1)	height (c_1)	length (a_2)	width (b_2)	height (c_1)
Size/μm	350	800	80	800	800	200

positive. Figure 3 and Figure 4 are the frame constructed. The beam's length, width and thickness are a_1, b_1 and c_1, respectively. The mass's length, width and thickness are a_2, b_2 and c_2, respectively. The size values are shown in Table 1. We simulated and analyzed the first four orders through ANSYS software. In Figure 3 and Figure 4: (a), (b), (c) and (d) are the first, second, third and fourth modes respectively. The first mode mass moves along the Z-axis, working as the working mode, the second mode mass rotates around the X-axis, the third mode mass rotates around the Y-axis, the fourth mode mass and frame move along the Z-axis.

The resonant frequencies of the four modes are shown in Table 2, which indicates that the 1st order mode resonant frequency is 408 kHz working as the working mode of HGMA. The 2nd order mode resonant frequency is 667 kHz and has 260 kHz gap with 1st mode, it means the coupling movement between these two modes is tiny, which is good for HGMA linearity.

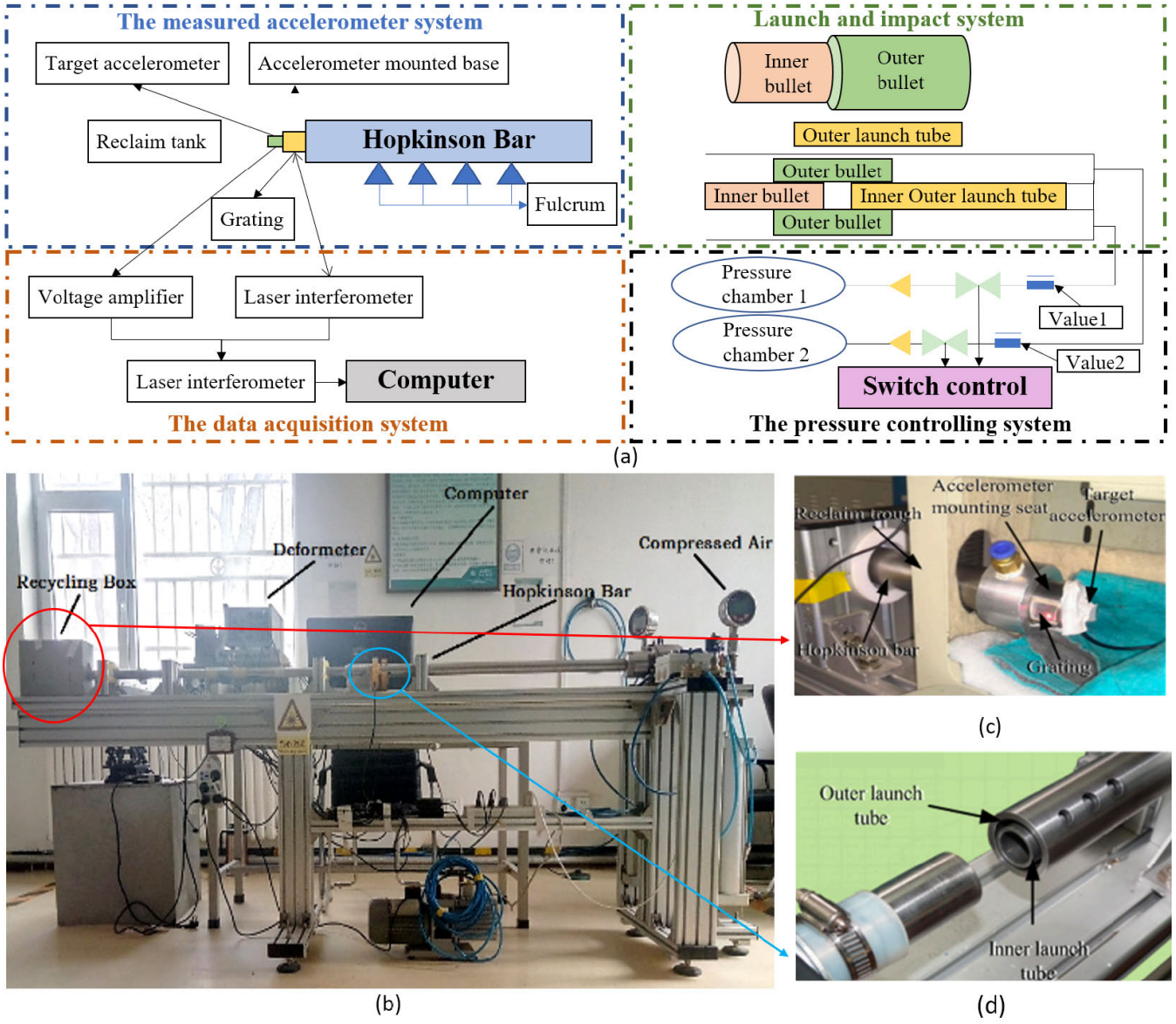

FIGURE 6. Hopkinson Bar calibration system.

TABLE 2. Resonant frequencies of the four modes.

Mode Shapes	1	2	3	4
Resonant Frequency /kHz	408	667	671	1119

Figure 5 shows the SEM photos and CCD photos of the accelerometer structure.

B. EXPERIMENT

The HGMA is calibrated in Hopkinson Bar calibration system as shown in Figure 6(b), and its output signal is also collected by the equipment, which is shown in Figure 6a. A power supply (GWINSTEK GPS-4303C) is employed to provide +5V voltage to HGMA, and a high-speed data acquisition system and a computer are employed to collect the HGMA output signal. Temperature is 25 °C (room temperature), and the sampling rate is 20MHz.

Figure 6 shows a schematic and experimental setup of a dynamic linear incremental impact system using a developed dual-warhead Hopkinson bar [8]. The impact measurement system includes a launch and impact system, a measured accelerometer system, a pressure control system and a data acquisition system, as shown in Figures 6(a), (b). Its launch tube and measured accelerometer are shown in Figures 6c, d respectively.

The accelerometer is mounted at the end of the base to measure the acceleration (1.5×10^5g $\sim 2.0 \times 10^5$g) caused by the bullet impacting the Hopkinson bar. To measure the pedestal Doppler shift due to acceleration, the grating is mounted next

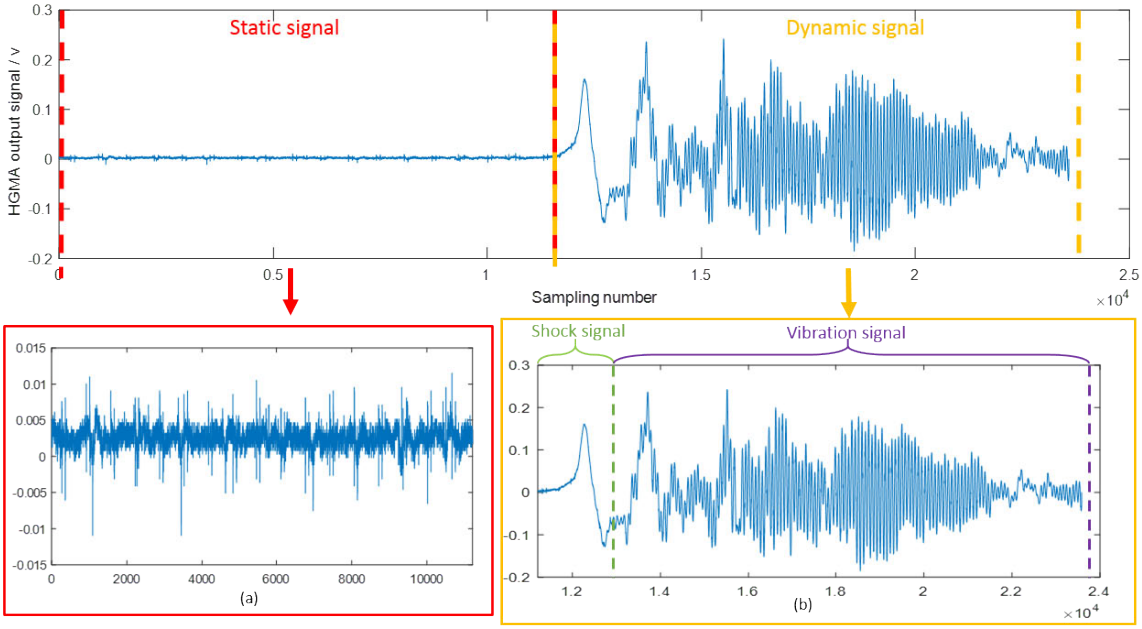

FIGURE 7. Signal decomposition result.

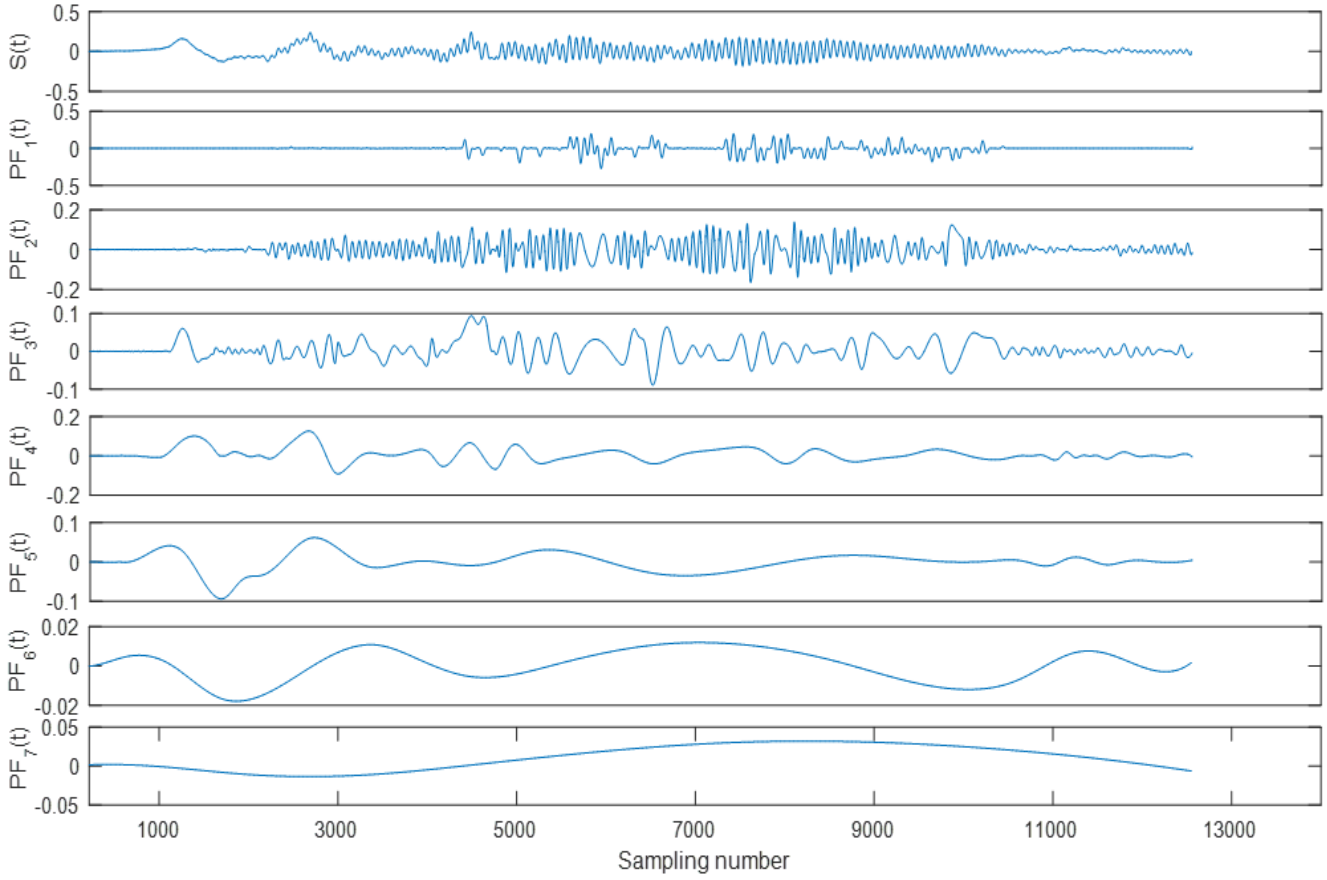

FIGURE 8. The results of LMD.

to the base. Pressure chambers 1 and 2 provide pressures up to 1 MPa. When we carry out the inner bullet (or external bullet) launch experiment, the inner (external) bullet hits the Hopkinson bar and produces a longitudinal elastic compression wave

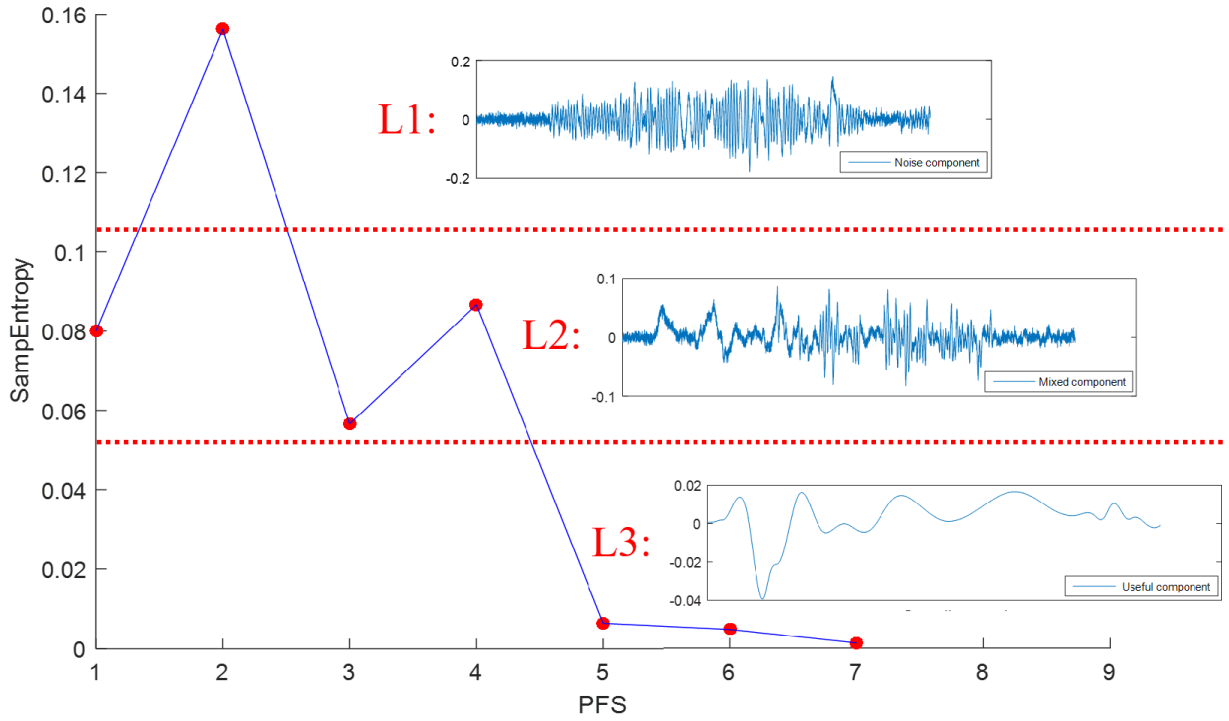

FIGURE 9. The calculation results of SE and classification results according to SE.

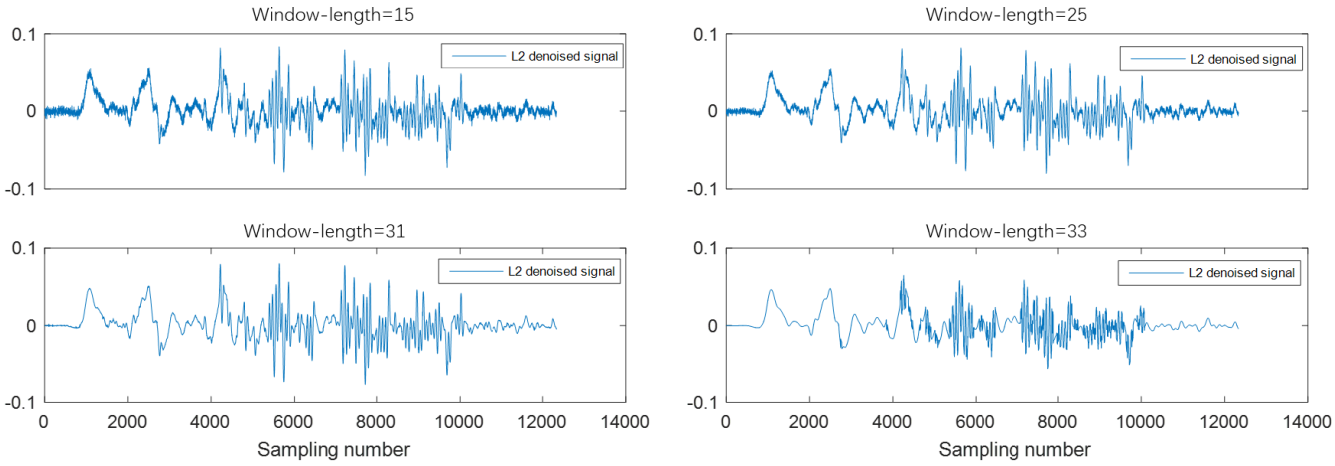

FIGURE 10. Denoising effect of different window length parameters.

on the other side. Due to the quasi-half-sine acceleration pulse from the compression wave, the accelerometer mounted on the side of the rod will immediately fly out.

The grating mounted on the pedestal measures the Doppler shift based on the accelerometer's acceleration and converts it into a voltage signal, it is ultimately input to the OP amplifier and analyzed by the data acquisition system.

When the accelerometer has no external interference and outputs a static signal, which contains rich random noise. We believe that the output signal at this stage can represent the statistical property of the noise in HGMA signal. When the sensor is subjected to external impact, the signal undergoes two stages of shock and vibration. The dynamic output signal contains both noise and useful signals. Figure 7 is the signal decomposition result, (a) is static signal, (b) is dynamic signal.

Through a large number of simulation experiments, we found that it would be more effective to denoise separately after dividing the test signal into static output and dynamic output.

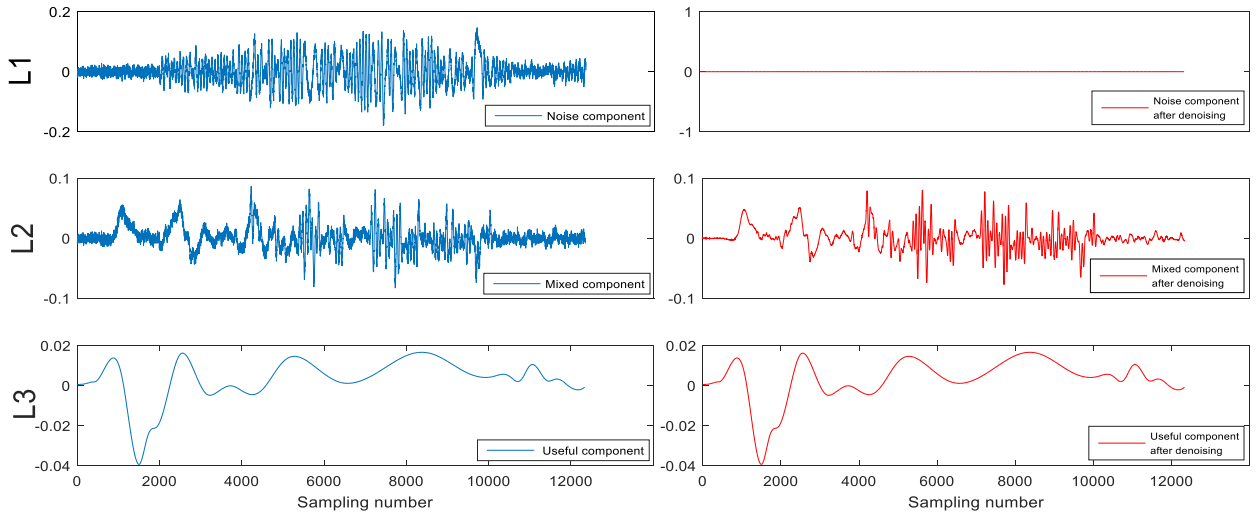

FIGURE 11. Noise reduction results of each layer.

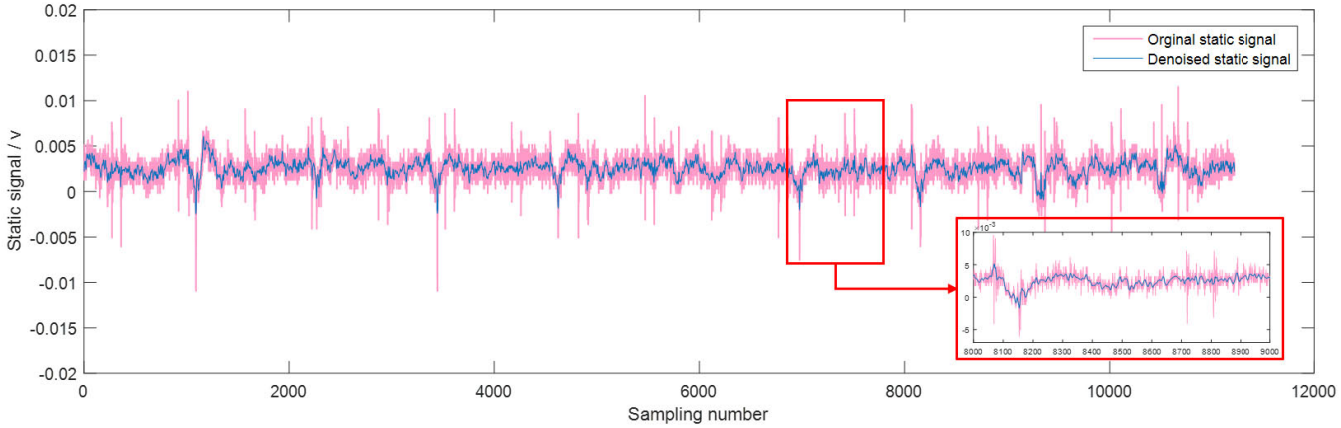

FIGURE 12. Static signal denoising results.

The algorithm demonstration part takes the noise reduction of the dynamic signal as an example, and the noise reduction of the static signal is similar to this, so we don't repeat it here.

According to the LMD-SE-TFPF algorithm, the first step is to perform a Local mean decomposition to the original signal. The output signal is decomposed into 7 PFs with different physical properties. Figure 8 is the result of LMD, S(t) is the original dynamic signal.

To calculate and classify the sample entropy of the PFs is the second step. Figure 9 shows the calculation result of the sample entropy value and the result of the signal classification. The Sample entropy value interval is 0∼0.16, and the calculated results are divided into three parts on average. PFs in the range of 0∼0.053 is considered as a useful component (L3: PF5∼PF7), the short-window TFPF is employed. PFs in the range of 0.053∼0.106 is considered as a mixed component (L2: PF1, PF3 and PF4), the long-window TFPF is employed. And noise component is in the range of 0.106∼0.16 (L1: PF2), which should be wiped off directly.

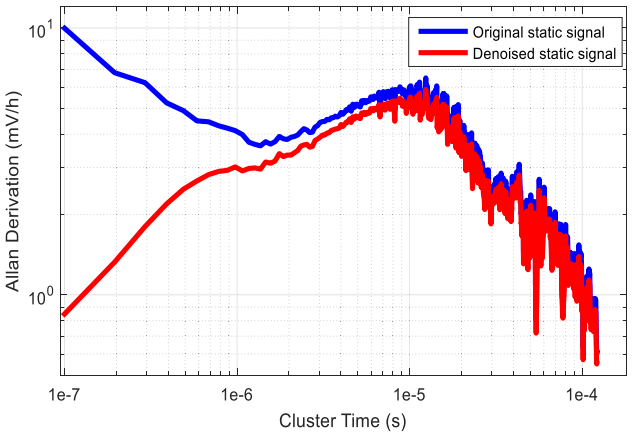

FIGURE 13. Allan derivation of the static signal denoising results.

When the window length parameter is gradually increased, as shown in Figure 10, the random noise reduction effect is getting better. When the window length is less than 17,

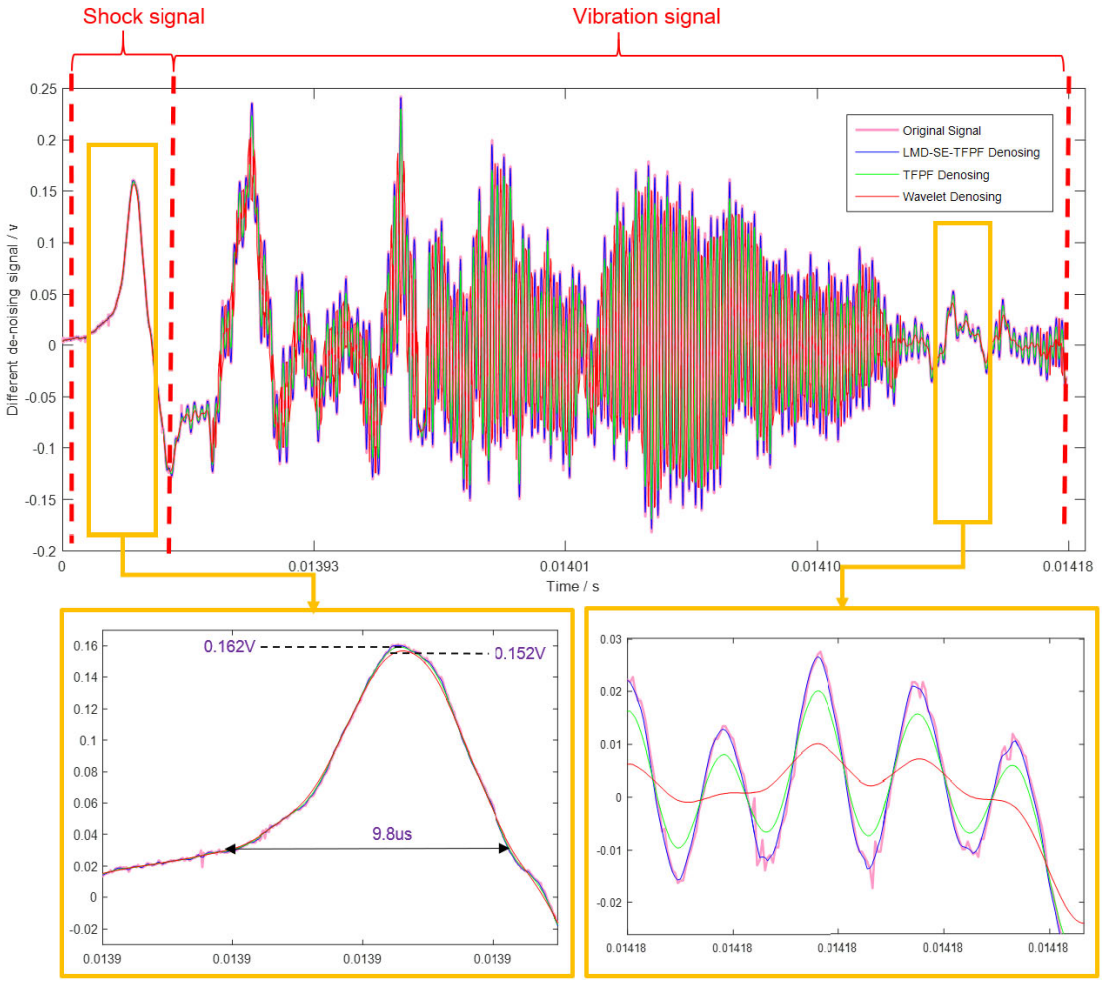

FIGURE 14. The comparison of different denoising algorithms for dynamic signal.

the effect of noise reduction is not obvious. When the window length is increased to 33, the signal is distorted, and the amplitude features do not match the original signal. At this time, 31 is the optimum long window length. For the useful component (L3), the signal characteristics should be preserved to the greatest extent, when the window length is 13 or 17, the signal is distorted. So, the short window length is chosen to be 7. It can be seen from Figure 11: the mixed component has a better denoising effect, as to the noise component, we remove it directly, the useful component retains the amplitude-frequency characteristic of the signal.

By superimposing the L2 signal and the L3 signal, we obtain the final denoised HGMA output signal.

IV. DISCUSSION

It is obvious in Figure 12 that the static signal contains rich noise (peak-to-peak is close to 0.013V) and the bias characteristics of the offset HGMA. The LMD-SE-TFPF method has obvious noise reduction effect on this part, this can be demonstrated by denoising results.

The Allan variance curve can not only represent the noise characteristics of the signal, but also quantitate the equivalent value of the acceleration random walking. Therefore, it is possible to check whether the signal noise level is reduced by the Allan variance analysis or not.

As shown in Figure 13, the value of original static signal and LMD-SE-TFPF denoising signals in 10^{-7} s are 10.1242mV/h and 0.8335 mV/h respectively. The noise of static signal is reduced by 91.76%, which can prove that the random noise of the signal is significantly reduced by the LMD-SE-TFPF method.

In order to compare the noise reduction effects of different methods, we performed separate TFPF denoising and traditional hard threshold wavelet denoising experiments to compare the noise reduction effects of different methods. Figure 14 is a comparison of the three methods. Dynamic signal is mainly divided into two stages: shock stage and vibration stage, we analyze the denoising effects of these two stages separately.

Shock stage: the main part of the calibration experiment, with a peak of about 0.162V and a pulse width of

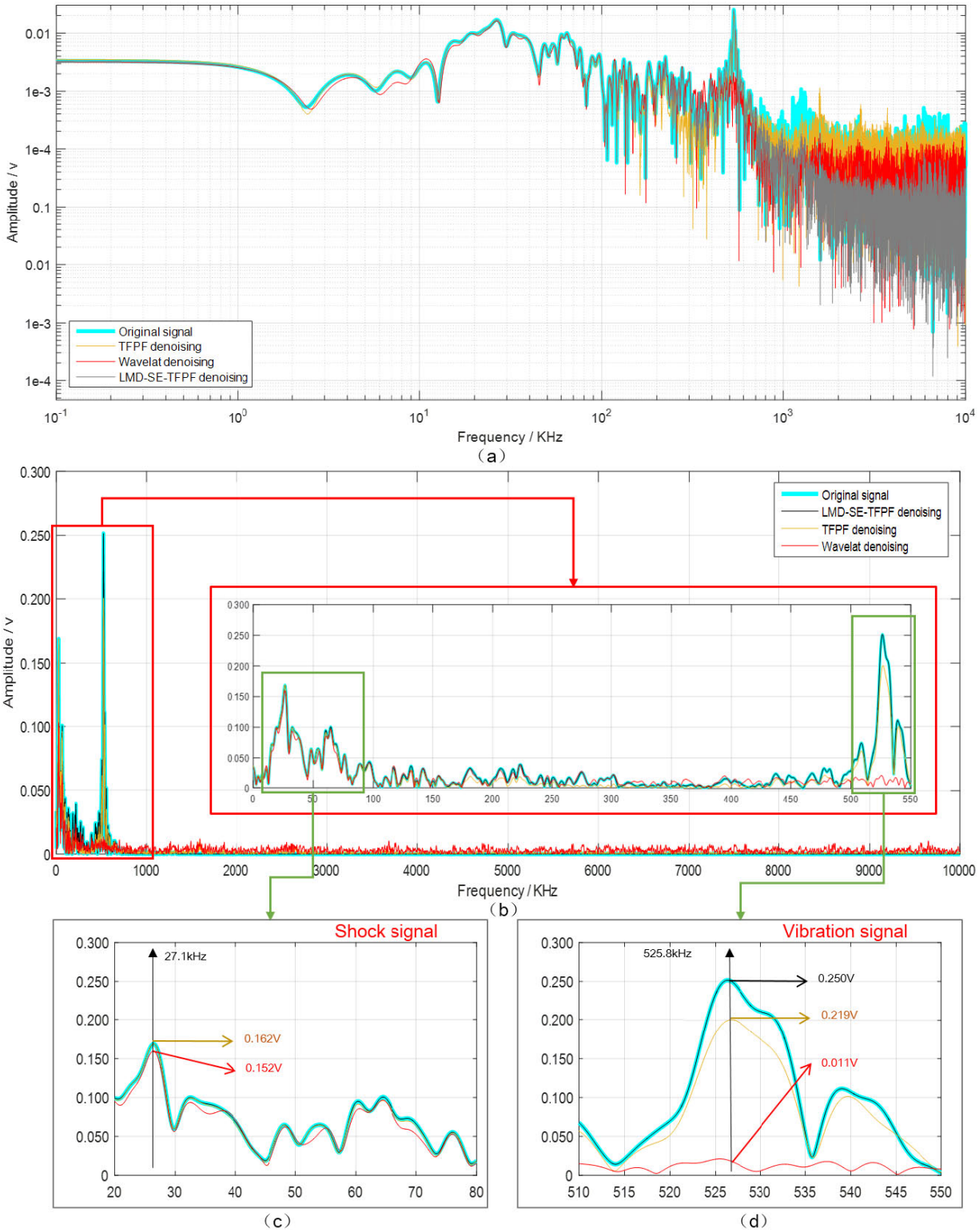

FIGURE 15. Frequency characteristic of dynamic signal and denoising results.

about 9.8μs. At this stage, the original signal data, the TFPF denoising signal and the LMD-SE-TFPF denoising signal almost overlap, indicating that the three curves contain the same information. However, the Wavelet denoising signal amplitude is 0.152V which is not well captured the original signal data, and the error is greater than 5%. Therefore, Wavelet denoising method is not suitable for calibration denoising.

TABLE 3. Parameter comparison of dynamic signal denoising by different methods.

Methods		Original signal	LMD-SE-TFPF	TFPF	Wavelet
Shock stage	Value / V	0.1621	0.1620	0.1618	0.1520
	Error from original	\	0.062%	0.123%	6.231%
Vibration stage	Value / V	0.2501	0.2500	0.2190	0.0110
	Error from original	\	0.04%	12.44%	95.60%

Vibration stage: this part mainly contains vibration information, which reflects the dynamic characteristics of HGMA. At this stage, it is clear that the Wavelet denoising signal has a serious distortion and cannot reflect the information of the original data. At the same time, after TFPF denoising, the amplitude decreases significantly and cannot represent the amplitude information of the original signal. Only the LMD-SE-TFPF method can capture the actual vibration signal.

The frequency characteristic of original signal and denoising results are shown in Figure 15. Figure 15a shows the frequency spectrum with a log-log scale, which can represent the noise statistic characteristic of HGMA output signal. It is obvious that the LMD-SE-TFPF method has the lowest noise. And the detailed analysis of the shock signal (Figure 15c) and the vibration signal (Figure 15d) are as follows:

Shock stage: the frequency peak of this phase is about 27.1 kHz. The original signal data, TFPF denoising signal and LMD-SE-TFPF denoising signal have almost the same amplitude (both around 0.162V). The amplitude of the Wavelet denoising result is 0.152V, and the signal is distorted. It shows that the LMD-SE-TFPF denoising method captures the actual amplitude and frequency information of the original signal.

Vibration stage: the frequency peak of the vibration phase is about 525.8 kHz. Since the sensor is vibrating along the Z axis, only the first mode of the sensor is excited. There is a deviation from the design value (408 kHz) caused by the machining error. From Figure 14d, we can conclude that the original signal data and the LMD-SE-TFPF denoising result have almost the same amplitude and shape (both around 0.250V). The TFPF denoising result has an amplitude of 0.219V and the error is 12.4%. The peak amplitude of the wavelet denoising result is 0.011V, and the signal attenuation is severe. It shows that TFPF and wavelet denoising are not suitable for the calibration denoising of the HGMA, only the LMD-SE-TFPF denoising method can capture the actual frequency information of the original signal. Based on the comprehensive performance of all aspects, the LMD-SE-TFPF method has a better denoising effect while maintaining the characteristics of the original signal.

Table 3 lists the denoising results of the three methods, as can be seen from Table 3, the LMD-SE-TFPF denoising algorithm is more effective in "Shock Stage" and "Vibration Stage". The LMD-SE-TFPF denoising algorithm errors in these two stages are 0.062% and 0.04% respectively, which is within the allowable range of calibration error.

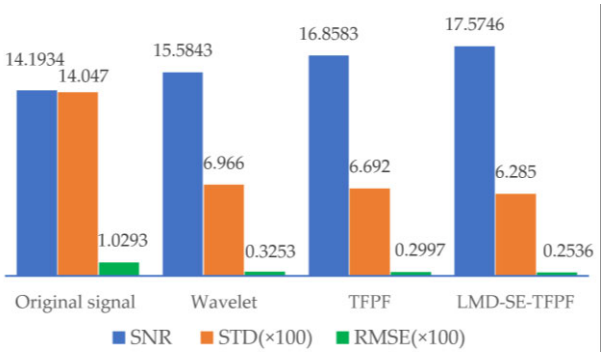

FIGURE 16. Parameter comparison of dynamic signal denoising by different methods.

What's more, this article evaluate the denoising method through three index: Signal-noise ratio (SNR), Standard deviation (STD) and Root mean square error (RMSE). Signal-noise ratio is the ratio of signal to noise in an electronic device or electronic system. The signal here refers to an electronic signal from outside which needs to be processed by this device. Noise is the additional irregular signals (or information) after passing through the device. The SNR is calculated as $10\lg(p_s/p_n)$, where p_s and p_n represent the effective power of the signal and noise respectively. It can also be converted into the ratio of the voltage amplitude: $20\lg(v_s/v_n)$, where v_s and v_n represent the effective value of signal and noise voltage. The STD can reflect the dispersion degree of the data, while the RMSE is used to measure the deviation between the observed value and the true value.

It is obvious from Figure 16 that the signal after the LMD-SE-TFPF algorithm has the highest signal to noise ratio (17.5746). At the same time, it has a low STD (0.06285) and RMSE (0.002536). From this we can make a conclusion that the LMD-SE-TFPF algorithm can reduce noise effectively.

V. CONCLUSION

This paper proposes a hybrid algorithm that combines TFPF with LMD and SE methods to reduce noise of High-G MEMS accelerometers signal. The window length of TFPF is adaptively selected by utilizing the decomposition characteristics of LMD and the value of SE, which highlights the advantages of each of the three algorithms. Compared with the traditional

TFPF and wavelet denoising, it breaks the limitation of the window length selection of the TFPF method. Experiments showed that this method can not only remove part of noise (the noise of static signal is reduced by 91.76%, the signal-noise ratio of dynamic signal has increased to 17.6) but also retain the details of frequency and amplitude (shock peak amplitude error is 0.062% and vibration characteristic amplitude error is 0.04%). Therefore, this method can improve the performance of High-G MEMS accelerometers which makes it widely used.

AUTHOR CONTRIBUTIONS

Z.Y., B.H. and J.T. conceived and designed the experiment; C.S., Y.S. and J.Z. manufactured the structure; H.C., J.L. and Z.Y. analyzed the data; H.C. and Z.Y. wrote the paper.

ACKNOWLEDGMENT

(Zeyu Yan and Chong Shen contributed equally to this work.)

CONFLICTS OF INTEREST

The authors declare no conflict of interest.

REFERENCES

[1] Y. Shi, R. Zhao, and J. Liu, "Design and testing of in-plane MEMS high-g accelerometer," *Appl. Mech. Mater.*, vols. 220–223, Nov. 2012, pp. 1857–1860.

[2] H. Cao, Y. Zhang, Z. Han, X. Shao, J. Gao, K. Huang, Y. Shi, J. Tang, C. Shen, and J. Liu, "Pole-zero temperature compensation circuit design and experiment for dual-mass MEMS gyroscope bandwidth expansion," *IEEE/ASME Trans. Mechatron.*, vol. 24, no. 2, pp. 677–688, Apr. 2019. doi: 10.1109/TMECH.2019.2898098.

[3] S. Chong, Z. Yu, T. Jun, C. Huiliang, and L. Jun, "Dual-optimization for a MEMS-INS/GPS system during GPS outages based on the cubature Kalman filter and neural networks," *Mech. Syst. Signal Process.*, to be published.

[4] H. Cao, Y. Liu, Y. Zhang, X. Shao, J. Gao, K. Huang, Y. Shi, J. Tang, C. Shen, and J. Liu, "Design and experiment of dual-mass MEMS gyroscope sense closed system based on bipole compensation method," *IEEE Access*, vol. 7, pp. 49111–49124, 2019.

[5] F. Liu, S. Gao, S. Niu, Y. Zhang, Y. Guan, C. Gao, and P. Li, "Optimal design of high-g MEMS piezoresistive accelerometer based on Timoshenko beam theory," *Microsyst. Technol.*, vol. 24, no. 2, pp. 855–867, 2018.

[6] H. Cao, Y. Liu, Z. Kou, Y. Zhang, X. Shao, J. Gao, K. Huang, Y. Shi, J. Tang, C. Shen, and J. Liu, "Design, fabrication and experiment of double U-beam MEMS vibration ring gyroscope," *Micromachines*, vol. 10, no. 3, p. 186, 2019.

[7] Y. Shi, Z. Yang, Z. Ma, H. Cao, Z. Kou, D. Zhi, Y. Chen, H. Feng, and J. Liu, "The development of a dual-warhead impact system for dynamic linearity measurement of a high-*g* micro-electro-mechanical-systems (MEMS) accelerometer," *Sensors*, vol. 16, no. 6, p. 840, 2016. doi: 10.3390/s16060840.

[8] Y. Shi, Y. Zhao, H. Feng, H. Cao, J. Tang, J. Li, R. Zhao, and J. Liu, "Design, fabrication and calibration of a high-G MEMS accelerometer," *Sensors Actuat. A, Phys.*, vol. 297, pp. 733–742, Aug. 2018.

[9] S. G. Chang, B. Yu, and M. Vetterli, "Adaptive wavelet thresholding for image denoising and compression," *IEEE Trans. Image Process.*, vol. 9, no. 9, pp. 1532–1546, Sep. 2000.

[10] H. Liu, W. Wang, C. Xiang, L. Han, and H. Nie, "A de-noising method using the improved wavelet threshold function based on noise variance estimation," *Mech. Syst. Signal Process.*, vol. 99, pp. 30–46, Jan. 2018.

[11] M. Safta, P. Svasta, and M.-O. Dima, "Wavelet signal denoising applied on electromagnetic traces," in *Proc. IEEE 23rd Int. Symp. Design Technol. Electron. Packag. (SIITME)*, Oct. 2017, pp. 399–402.

[12] C. Pang, S. Liu, and H. Yan, "High-speed target detection algorithm based on sparse Fourier transform," *IEEE Access*, vol. 6, pp. 37828–37836, 2018.

[13] A. O. Boudraa and J. C. Cexus, "EMD-based signal filtering," *IEEE Trans. Instrum. Meas.*, vol. 56, no. 6, pp. 2196–2202, Dec. 2007.

[14] Y. Xue, J. Zhang, Q. Chang, L.-P. Zhang, and F. Zou, "Instantaneous frequency extraction using the EMD-based wavelet ridge to reveal geological features," *Frontiers Earth Sci.*, vol. 6, p. 65, May 2018.

[15] C. Shen, H. Cao, J. Li, J. Tang, X. Zhang, Y. Shi, W. Yang, and J. Liu, "Hybrid de-noising approach for fiber optic gyroscopes combining improved empirical mode decomposition and forward linear prediction algorithms," *Rev. Sci. Instrum.*, vol. 87, no. 3, 2016, Art. no. 033305.

[16] Y. Wang, Z. He, and Y. Zi, "A comparative study on the local mean decomposition and empirical mode decomposition and their applications to rotating machinery health diagnosis," *J. Vibrat. Acoust.*, vol. 132, no. 2, Mar. 2010, Art. no. 021010.

[17] L. Wang, Z. Liu, Q. Miao, and X. Zhang, "Time–frequency analysis based on ensemble local mean decomposition and fast kurtogram for rotating machinery fault diagnosis," *Mech. Syst. Signal Process.*, vol. 103, pp. 60–75, Mar. 2018.

[18] Z. Liu, X. Chen, Z. He, and Z. Shen, "LMD method and multi-class RWSVM of fault diagnosis for rotating machinery using condition monitoring information," *Sensors*, vol. 13, no. 7, pp. 8679–8694, Jul. 2013.

[19] L. Bai, Z. Han, Y. Li, and S. Ning, "A hybrid de-noising algorithm for the gear transmission system based on CEEMDAN-PE-TFPF," *Entropy*, vol. 20, no. 5, p. 361, 2018.

[20] Y. Liu, L. Yue, P. Nie, and Qian Zeng, "Spatiotemporal time–frequency peak filtering method for seismic random noise reduction," *IEEE Geosci. Remote Sens. Lett.*, vol. 10, no. 4, pp. 756–760, Jul. 2013.

[21] S. Ning, Z. Han, Z. Wang, and X. Wu, "Application of sample entropy based LMD-TFPF de-noising algorithm for the gear transmission system," *Entropy*, vol. 18, no. 11, p. 414, 2016.

[22] Z. Wang, J. Zhou, J. Wang, W. Du, J. Wang, X. Han, and G. He, "A novel fault diagnosis method of gearbox based on maximum kurtosis spectral entropy deconvolution," *IEEE Access*, vol. 7, pp. 29520–29532, 2019. doi: 10.1109/ACCESS.2019.2900503.

[23] C. Shen, X. Liu, H. Cao, Y. Zhou, J. Liu, J. Tang, X. Guo, H. Huang, and X. Chen, "Brain-like navigation scheme based on MEMS-INS and place recognition," *Appl. Sci.*, vol. 9, no. 8, p. 1708, 2019.

[24] Z. Wang, J. Wang, and W. Du, "Research on fault diagnosis of gearbox with improved variational mode decomposition," *Sensors*, vol. 18, no. 10, p. 3510, 2018.

[25] Z.-X. Yang and J.-H. Zhong, "A hybrid EEMD-based SampEn and SVD for acoustic signal processing and fault diagnosis," *Entropy*, vol. 18, no. 4, pp. 112, 2016.

[26] D. Xiang and S. Ge, "Method of fault feature extraction based on EMD sample entropy and LLTSA," *J. Aerosp. Power*, vol. 29, no. 7, pp. 1535–1542, 2014.

[27] Z. Wang, W. Du, J. Wang, J. Zhou, X. Han, Z. Zhang, and L. Huang, "Research and application of improved adaptive MOMEDA fault diagnosis method," *Measurement*, vol. 140, pp. 63–75, Jul. 2019.

[28] Z. Wang, G. He, W. Du, J. Zhou, X. Han, J. Wang, H. He, X. Guo, J. Wang, and Y. Kou, "Application of parameter optimized variational mode decomposition method in fault diagnosis of gearbox," *IEEE Access*, vol. 7, pp. 44871–44882, 2019. doi: 10.1109/ACCESS.2019.2909300.

[29] J. Lv and J. Yu, "Average combination difference morphological filters for fault feature extraction of bearing," *Mech. Syst. Signal Process.*, vol. 100, pp. 827–845, Feb. 2018.

[30] Z. Hu, C. Wang, J. Zhu, X. Liu, and F. Kong, "Bearing fault diagnosis based on an improved morphological filter," *Measurement*, vol. 80, pp. 163–178, Feb. 2016.

[31] Q. Lu, L. Pang, H. Huang, C. Shen, H. Cao, Y. Shi, and J. Liu, "High-G calibration denoising method for High-G MEMS accelerometer based on EMD and wavelet threshold," *Micromachines*, vol. 10, no. 2, p. 134, 2019.

[32] X. Xu, M. Luo, Z. Tan, and R. Pei, "Echo signal extraction method of laser radar based on improved singular value decomposition and wavelet threshold denoising," *Infr. Phys. Technol.*, vol. 92, pp. 327–335, Aug. 2018.

[33] F. Bi, T. Ma, and X. Wang, "Development of a novel knock characteristic detection method for gasoline engines based on wavelet-denoising and EMD decomposition," *Mech. Syst. Signal Process.*, vol. 117, pp. 517–536, Feb. 2019.

[34] C. Shen, J. Yang, J. Tang, J. Liu, and H. Cao, "Note: Parallel processing algorithm of temperature and noise error for micro-electro-mechanical system gyroscope based on variational mode decomposition and augmented nonlinear differentiator," *Rev. Sci. Instrum.*, vol. 89, no. 7, 2018, Art. no. 076107.

[35] Z. Wang, J. Wang, W. Cai, J. Zhou, W. Du, J. Wang, G. He, and H. He, "Application of an improved ensemble local mean decomposition method for gearbox composite fault diagnosis," *Complexity*, vol. 2019, May 2019, Art. no. 1564243. doi: 10.1155/2019/1564243.
[36] H. Cao, Y. Zhang, C. Shen, Y. Liu, and X. Wang, "Temperature energy influence compensation for MEMS vibration gyroscope based on RBF NN-GA-KF method," *Shock Vib.*, vol. 2018, Dec. 2018, Art. no. 2830686.
[37] Z. Wang, L. Zheng, W. Du, W. Cai, J. Zhou, J. Wang, X. Han, and G. He, "A novel method for intelligent fault diagnosis of bearing based on capsule neural network," *Complexity*, vol. 2019, Jun. 2019, Art. no. 6943234. doi: 10.1155/2019/6943234.
[38] L. Zhao, S. Wei, C. Zhang, Y. Zhang, X. Jiang, F. Liu, and C. Liu, "Determination of sample entropy and fuzzy measure entropy parameters for distinguishing congestive heart failure from normal sinus rhythm subjects," *Entropy*, vol. 17, no. 12, pp. 6270–6288, 2015.
[39] W. Yue, P. Shang, and Y. Li, "Modified generalized multiscale sample entropy and surrogate data analysis for financial time series," *Nonlinear Dyn.*, vol. 92, no. 3, pp. 1335–1350, 2018.
[40] C. Shen, J. Li, X. Zhang, J. Tang, H. Cao, and J. Liu, "Multi-scale parallel temperature error processing for dual-mass MEMS gyroscope," *Sens. Actuators A, Phys.*, vol. 245, pp. 160–168, Jul. 2016.
[41] W. Choi, M. B. Pate, and J. F. Sweeney, "Uncertainty and signal-to-noise ratio for unsteady background noise," *Noise Control Eng. J.*, vol. 66, no. 2, pp. 131–141, 2018.
[42] H. Huang, X. Chen, B. Zhang, and J. Wang, "High accuracy navigation information estimation for inertial system using the multi-model EKF fusing adams explicit formula applied to underwater gliders," *ISA Trans.*, vol. 66, pp. 414–424, Jan. 2017.
[43] H. Huang, J. Zhou, J. Zhang, Y. Yang, R. Song, J. Chen, and J. Zhang, "Attitude estimation fusing Quasi-Newton and cubature Kalman filtering for inertial navigation system aided with magnetic sensors," *IEEE Access*, vol. 6, pp. 28755–28767, 2018.

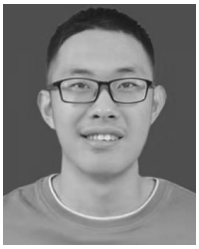

ZEYU YAN is currently pursuing the bachelor's degree with the School of Instrument and Electronics, North University of China, Taiyuan, Shanxi, China. His research interests include MEMS device test and data analysis.

BOYANG HOU is currently pursuing the bachelor's degree with the Glasgow College, University of Electronic Science and Technology of China, Chengdu, China. His research interests include MEMS device test and data analysis.

JINGCHUN ZHANG is currently pursuing the degree with the Beijing Huijia Private School, Beijing, China. Her research interest includes MEMS device design and test.

CHONG SHEN received the Ph.D. degree in instrument science and technology from Southeast University, Nanjing, China, in 2013. He is currently an Associate Professor with the School of Instrument and Electronics, North University of China, Taiyuan, Shanxi, China. His research interests include MEMS inertial devices de-noising and inertial guidance system design.

YUNBO SHI received the B.S. and M.S. degrees from the North University of China, Shanxi, China, in 1995 and 2003, respectively, and the Ph.D. degree from the Beijing Institute of Technology of China, in 2014. He is currently a Professor with the North University of China. His research interests include measurement, semiconductor materials, and devices.

JUN TANG received the B.S. degree from the North University of China, Taiyuan, China, in 2003 and 2006, respectively, and the Ph.D. degree from the National Technical University of Athens, Athens, Greece, in 2010. He has been a Professor with the North University of China, since 2016. His research interests include micro electromechanical systems inertial sensor and nano phase materials.

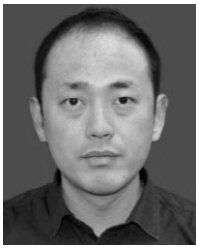

HUILIANG CAO (M'18) received the Ph.D. degree in instrument science and technology from Southeast University, Nanjing, China, in 2014. From 2011 to 2012, he was a Research Ph.D. Student with the School of Electrical and Computer Engineering, Georgia Institute of Technology, Atlanta, USA. He is one of the Top Young Academic Leaders of Higher Learning Institutions of Shanxi and Young Academic Leaders of North University of China. He is currently a Postgraduate Tutor and a Professor with the School of Instrument and Electronics, North University of China, Taiyuan, Shanxi, China. His research interest includes MEMS inertial devices.

JUN LIU received the Ph.D. degree from the Beijing Institute of Technology, Beijing, China, in 2001. From 2001 to 2005, he was a Postdoctoral Researcher with Peking University. He is currently a Distinguished Professor with the North University of China, Taiyuan, China. His current research interests include intelligent instrument, micro inertia devices, and micro electromechanical systems devices.